





Evidence of unconventional vortex states in the Chevrel phase superconductor PbMo_6Se_8

Souvik Banerjee , Sudip Ghosh , Anshu Kataria , and A. Sundaresan *
*Chemistry and Physics of Materials Unit, School of Advanced Materials,
 Jawaharlal Nehru Centre for Advanced Scientific Research, Bengaluru 560064, India*



(Received 2 August 2023; revised 16 May 2024; accepted 28 June 2024; published 15 July 2024)

We present a comprehensive investigation of superconducting properties in the Chevrel phase compound PbMo_6Se_8 by x-ray diffraction, dc magnetization, resistivity, heat capacity, and magnetic relaxation experiments. We determine a bulk superconducting transition temperature T_c of 3.8 K. Key superconducting parameters such as lower $[\mu_0 H_{c1}(0)]$ and upper $[\mu_0 H_{c2}(0)]$ critical fields, coherence length $[\xi_{\text{GL}}(0)]$, penetration depth $[\lambda_{\text{GL}}(0)]$, Ginzburg-Landau parameter (κ), Pauli paramagnetic field ($\mu_0 H_p^{\text{st}}$), and Maki parameter (α_M) are obtained. The BCS model provides a reasonable description of the heat-capacity data. An unconventional vortex state is evident from the investigation of the unusual fishtail effect and nonmonotonous magnetic field dependency of the vortex pinning energy obtained from the magnetic relaxation experiments, indicating a deviation from the ideal type II superconducting vortex, in PbMo_6Se_8 . A detailed $\mu_0 H$ -T phase diagram has been drawn illustrating a multiphase vortex crossover.

DOI: [10.1103/PhysRevB.110.014512](https://doi.org/10.1103/PhysRevB.110.014512)

I. INTRODUCTION

The Chevrel phases, discovered in 1970, represent a captivating group of materials distinguished by their unique crystal structure and fascinating superconducting properties [1]. These materials are generally denoted by the formula $A_x\text{Mo}_6X_8$ (A = monovalent or divalent or trivalent cation, x = chalcogenides S, Se, Te; the specific value of x varies from 0 to 4 depending on the charge and the ionic radii of the cation) [1,2]. During 1975–1976, superconductivity was observed in RMo_6S_8 and RMO_6Se_8 , where R is the rare-earth atom [3]. The coexistence of ferromagnetic order and the reentrant nature of superconductivity was reported in ErRh_4B_4 and HoMo_6S_8 [3,4]. PbMo_6S_8 and SnMo_6S_8 were identified as high-field superconductors (SCs) with a critical field of ≈ 60 T, making them potential alternatives to Nb-Sn superconductors in practical applications [3–9]. However, with the discovery of high- T_c cuprates in the 1980s, the study and characterization of these intriguing Chevrel phases remained incomplete but still relevant [10]. In 2007, Fischer’s group observed nodelike excitations in the superconducting gap structures of the Chevrel phase compound PbMo_6S_8 . A few years later, in 2011, the same group confirmed the existence of multi-gap superconductivity in both PbMo_6S_8 and SnMo_6S_8 using scanning tunneling spectroscopy [11,12]. Despite sharing a common structural identity, the different materials within this family exhibit diverse superconducting properties, necessitating a comprehensive investigation into the superconducting properties of each member.

PbMo_6S_8 stands out among the Chevrel phase compounds as one of the extensively studied systems due to its remarkable critical temperature (T_c) and critical magnetic field ($\mu_0 H_{c2}$). However, the corresponding selenium compound PbMo_6Se_8

has received limited attention regarding its superconducting properties. This lack of comprehensive investigation motivated us to conduct a detailed and systematic study on the superconducting characteristics of PbMo_6Se_8 using various techniques such as x-ray diffraction, magnetization, resistivity, heat capacity, and magnetic relaxation measurements. The BCS theory gives a reasonable description of the heat-capacity data. Notably, we have observed a fishtail effect in isothermal magnetization in a three-dimensional (3D) crystal lattice which is quite rare and has been observed earlier in quasi-2D Fe-based SCs and high- T_c cuprates SCs, indicating an unconventional superconducting vortex state. A detailed multivortex superconducting phase diagram has been established from all the magnetic and resistivity measurements.

II. EXPERIMENTAL DETAILS

Polycrystalline samples of PbMo_6Se_8 were synthesized by the conventional solid-state method from elemental Pb (99.99%), Mo (99.99%), and Se (99.99%) in an evacuated silica tube of pressure less than 10^{-4} torr as reported earlier [10]. The phase purity and crystal structure of the samples were confirmed through Rietveld refinement analysis using x-ray diffraction data (XRD), obtained from a PANalytical diffractometer with $\text{Cu } K\alpha_1$ radiation. The refinement was carried out using FULLPROF software [13] indicating the samples crystallizing in rhombohedral structure which is consistent with an earlier report [14]. Magnetic measurements were carried out using Magnetic Properties Measurement System (MPMS), Quantum Design, USA. The electrical transports and specific heat were measured with Physical Properties Measurement System (PPMS), Quantum Design, USA. A conventional four-probe method and time relaxation technique were used for electrical transport (resistivity measurements) and heat capacity, respectively. Magnetization measurements were carried out in a rectangular pellet of dimension

*Contact author: sundaresan@jncasr.ac.in

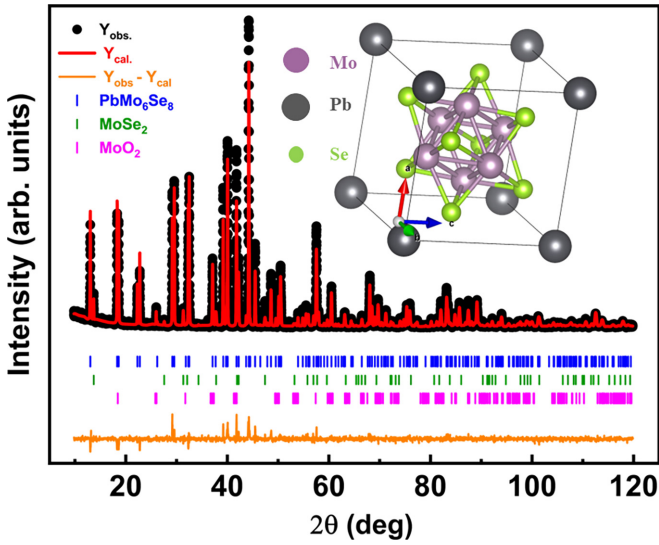


FIG. 1. Rietveld refinement of room-temperature powder XRD data with $\approx 1\%$ MoSe_2 and 5% MoO_2 phase. Inset shows obtained crystal structure of rhombohedral PbMo_6Se_8 phase with Mo_6Se_8 cluster inside the structure with Pb atoms at the corner.

$\approx 6 \text{ mm} \times 2 \text{ mm} \times 0.6 \text{ mm}$ with an external applied magnetic field perpendicular to the breadth of dimension 2 mm . Electrical resistivity was measured in a rectangular pellet of dimension $5.4 \text{ mm} \times 1.9 \text{ mm} \times 1.1 \text{ mm}$ with 1 mA current. Heat capacity was performed in a pellet of smooth surface with a weight of 6 mg . Magnetic relaxation measurements

were carried out in the following protocol: after cooling down the system from a normal state to a superconducting state in the absence of any externally applied magnetic field, we apply the magnetic field and start recording the magnetic moment with time in MPMS, Quantum Design, USA.

III. RESULTS AND DISCUSSIONS

A. Structural characterization

The Rietveld refinement suggests that PbMo_6Se_8 crystallizes in rhombohedral $R\bar{3}$ structure (space group no. 148), which is consistent with earlier reports [10,14]. The rhombohedron of length $6.7968(1) \text{ \AA}$ and angle $89.107(2)^\circ$ consists of Pb atoms located at the corners and one Mo_6Se_8 cluster inside, as shown in the inset of Fig. 1. The identifiable impurity phases are MoO_2 ($\approx 5\%$) and MoSe_2 ($\approx 1\%$).

B. Magnetization and resistivity

The temperature-dependent volume susceptibility, measured under a magnetic field of 1 mT , is illustrated in Fig. 2(a). The results indicate a sharp superconducting transition starting at $T_c^{\text{onset}} = 4.2 \text{ K}$ and ending at $T_c^{\text{full}} = 3.6 \text{ K}$ with a width of $\Delta T_c^m = 0.60 \text{ K}$ along with a high ratio of $\frac{T_c}{\Delta T_c} \approx 7$. Furthermore, the volume susceptibility, measured using the zero-field-cooled (ZFC) protocol with a magnetic field of 1 mT , is found to be 0.88 after considering the demagnetization correction [15]. This observation suggests that 88% of the volume of the system exhibits superconductivity at the lowest achievable temperature of 1.9 K . Importantly, this value

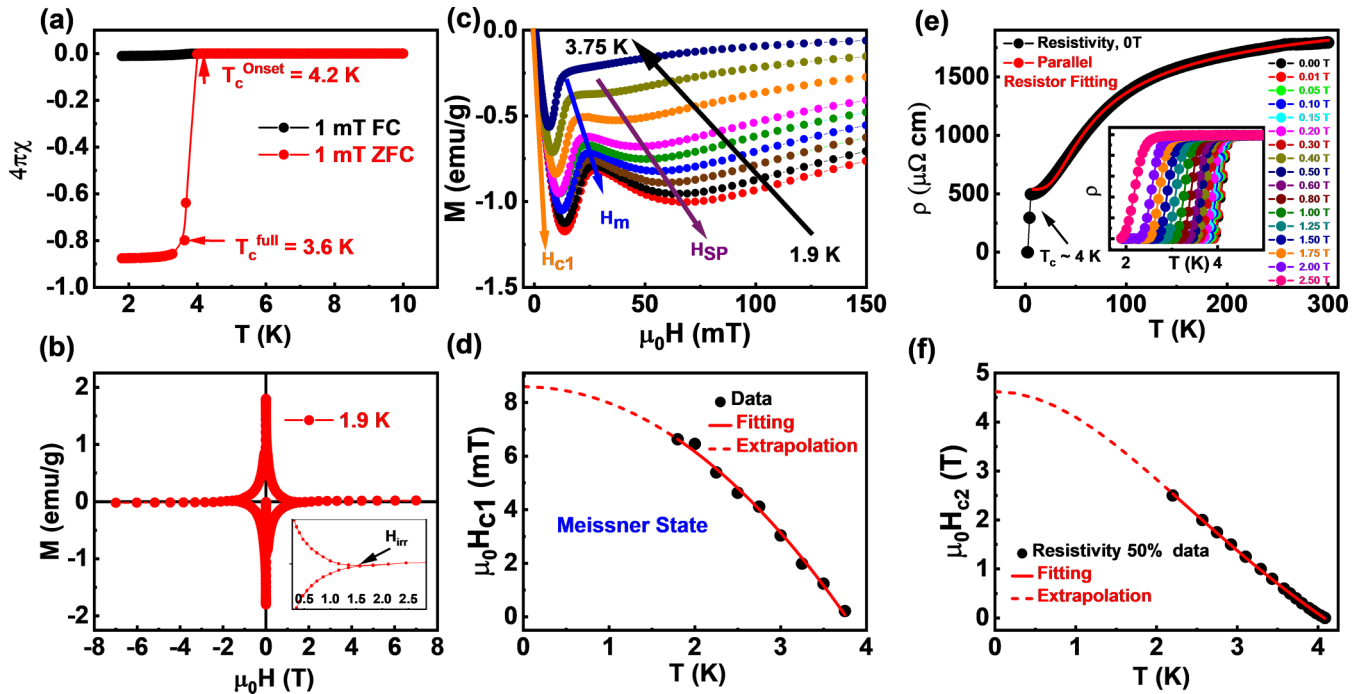


FIG. 2. (a) Volume susceptibility after demagnetization correction measured at 1 mT . (b) Isothermal magnetization at 1.9 K . Inset shows the same in expanded scale. (c) Evolution of magnetic isotherms from 1.9 to 3.75 K . Observation of two magnetic anomalies called H_m and H_{SP} and their shift with temperature. (d) Fitting of lower critical field (H_{c1}) from isothermal magnetization. (e) Temperature-dependent resistivity and associated parallel resistor model fit. Magnetic field dependence of superconducting transition in resistivity data in the inset. (f) Fitting of upper critical field (H_{c2}) from Ginzburg-Landau theory from 50% drop of resistivity data.

closely aligns with the phase fraction of the superconducting phase PbMo_6Se_8 obtained from the Rietveld refinement, which was found to be 0.94. We performed isothermal magnetization measurements at various temperatures ranging from 1.9 to 3.5 K, as illustrated in Figs. 2(b) and 2(c). From the isotherms depicted in Fig. 2(c) we have obtained the lower critical field $\mu_0 H_{c1}(T)$ and fitted the T dependency [16] with the following equation:

$$\mu_0 H_{c1}(T) = \mu_0 H_{c1}(0)(1 - t^2), \quad (1)$$

where $t = \frac{T}{T_c}$ and $\mu_0 H_{c1}(0)$ is the lower critical field at absolute zero, and T_c is the superconducting temperature obtained from fitting. We obtained $\mu_0 H_{c1}(0) = 8.588 \pm 0.146$ mT and $T_c = 3.77 \pm 0.03$ K. Interestingly, the magnetization isotherm in Fig. 2(c) exhibits two anomalies above $\mu_0 H_{c1}$, shown in Fig. 2(c), named the minimum ($\mu_0 H_m$) and the secondary peak ($\mu_0 H_{SP}$). This phenomenon is referred to as the fishtail effect in superconductors, mostly observed in high- T_c cuprates and Fe-based superconductors [16–19]. The origin of the fishtail effect is related to the complex interplay between superconductivity, magnetic field penetration, and the behavior of vortices within the material. It is influenced by factors such as the presence of competing order parameters, the presence of defects, and the intricate interplay between superconductivity and magnetism in these materials. However, irrespective of origin, it is extremely rare to find a material other than cuprates and the Fe-based SC family to exhibit such phenomena. A detailed discussion of this unconventional vortex state will be presented in the upcoming section.

The temperature-dependent resistivity in the absence of an applied magnetic field is illustrated in Fig. 2(e). It demonstrates a clear superconducting transition at temperature T_c^R (50% drop) = 4.11 K with a width of $\Delta T_c^R = 0.24$ K suggesting a sharp superconducting transition with the ratio of $\frac{T_c^R}{\Delta T_c^R} \approx 17$. We obtained a value of resistivity $\rho_{6.5\text{ K}} \approx 493$ $\mu\Omega$ cm indicating poor metallic behavior. The residual resistivity ratio (RRR), $\frac{\rho_{300\text{ K}}}{\rho_{6.5\text{ K}}}$, is found to be ≈ 3.65 , which suggests significant defect scattering at low temperature. At $T > 100$ K the resistivity exhibits a flattening trend with temperature, a characteristic commonly observed in superconductors based on d -block elements [20]. Such saturation can be explained by the parallel resistor model [21,22] described by the following equation:

$$\rho(T) = \left(\frac{1}{\rho_{\text{sat}}} + \frac{1}{\rho_{\text{ideal}}(T)} \right)^{-1}, \quad (2)$$

where ρ_{sat} is the saturated resistivity at higher temperatures and independent of temperature T , and $\rho_{\text{ideal}}(T)$ can be written as Matthiessen's rule given by the following equation:

$$\rho_{\text{ideal}}(T) = \rho_{\text{ideal},0} + \rho_{\text{ideal},L}(T), \quad (3)$$

where $\rho_{\text{ideal},0}$ is the residual resistivity which is temperature-independent, and $\rho_{\text{ideal},L}(T)$ is the temperature-dependent term expressed by the generalized Bloch-Gruneisen model [20]. The $\rho_{\text{ideal}}(T)$ after this Bloch - Gruneisen approximation can be written as $\rho_G(T)$ given by the following equation:

$$\rho_G(T) = \rho_{\text{ideal},0} + C \left(\frac{T}{\theta_R} \right)^n \int_0^{\frac{\theta_R}{T}} \frac{x^n}{(e^{-x} + 1)(e^x - 1)} dx, \quad (4)$$

where θ_R is the Debye temperature obtained from resistivity measurements, and C is a material-dependent constant, $n = 3$ or 5, depending on the mode of scattering. We obtained a best fit with $n = 3$ which accounts for umklapp's scattering between bands [20]. We obtained $\rho_{\text{sat}} = 2128.52 \pm 4.27$ $\mu\Omega$ cm, $C = 19120.55 \pm 356.61$ $\mu\Omega$ cm, $\theta_R = 244.11 \pm 2.47$ K. The calculated residual resistivity $\rho_0 = \frac{\rho_{\text{sat}} \rho_{\text{ideal},0}}{\rho_{\text{sat}} + \rho_{\text{ideal},0}}$ turns out to be $\rho_0 = 522.2 \pm 0.4$ $\mu\Omega$ cm, which is close to the experimental value of ≈ 493 $\mu\Omega$ cm. The electrical resistivity of our sample is similar to the data of $\text{Cu}_x\text{Mo}_6\text{S}_{8-y}\text{Se}_y$ [23]. To calculate the upper critical field H_{c2} , we have measured field-dependent resistivity in several different magnetic fields of 0, 0.01, 0.05, 0.10, 0.15, 0.20, 0.30, 0.40, 0.50, 0.60, 0.80, 1.00, 1.25, 1.50, 1.75, 2.00, and 2.50 T shown in Fig. 2(e), inset. Taking the point of 50% drop of normal resistivity as T_c , we have plotted $\mu_0 H_{c2}$ versus T in Fig. 2(f) and fitted with the Ginzburg-Landau model [24] according to the following equation:

$$\mu_0 H_{c2}(T) = \mu_0 H_{c2}(0) \frac{1 - t^2}{1 + t^2} \quad (5)$$

obtaining $\mu_0 H_{c2}(0) = 4.62 \pm 0.02$ T and $T_c = 4.08 \pm 0.01$ K.

C. Heat capacity

The superconductivity of PbMo_6Se_8 was further investigated using temperature-dependent heat-capacity measurements. The presence of a bulk superconducting transition is evident from the anomaly at $T_c \approx 3.75$ K of specific-heat data shown in the inset of Fig. 3(a). The whole range plot of $\frac{C_p}{T}$ versus T^2 shows a saturation kind of behavior that deviates much from a linearized version of low-temperature $\frac{C_p}{T}$ versus T^2 plot suggesting a possibility of the presence of low-energy soft phonon modes in the system. However, before looking into any low-energy phonon modes in it, it is essential to find out the Sommerfeld coefficient correctly from the linearized portion of $\frac{C_p}{T}$ versus T^2 plot by the following equation [25]: $\frac{C_p}{T} = \gamma + \beta T^2 + \delta T^4$, typically valid for $T \ll \theta_D$, where γ represents the electronic contribution to the specific heat, known as the Sommerfeld coefficient, and β and δ are the phonon contribution. It is important to note that the Sommerfeld coefficient obtained from whole range fitting considering the low-energy Einstein modes often leads to the incorrect value, and this is because of the huge differences in energy scale between the Sommerfeld coefficient and the existing Einstein modes [26]. We obtained a value of $\gamma = 31.56 \pm 6.13$ mJ mol⁻¹ K⁻² from the above equation fitted in the linear region from 4 to 6 K. Previous studies have predicted that Chevrel phase compounds, such as PbMo_6S_8 , exhibit low-energy soft phonon modes [27]. Consequently, it is anticipated that at low temperatures, the specific heat of PbMo_6Se_8 will be influenced by these low-lying Einstein modes as well, leading to perturbations in its low-temperature specific-heat behavior. Considering the prediction for the isostructural PbMo_6S_8 [27], to get to know about low-energy excitations or soft phonon modes we have used the following equation to fit the

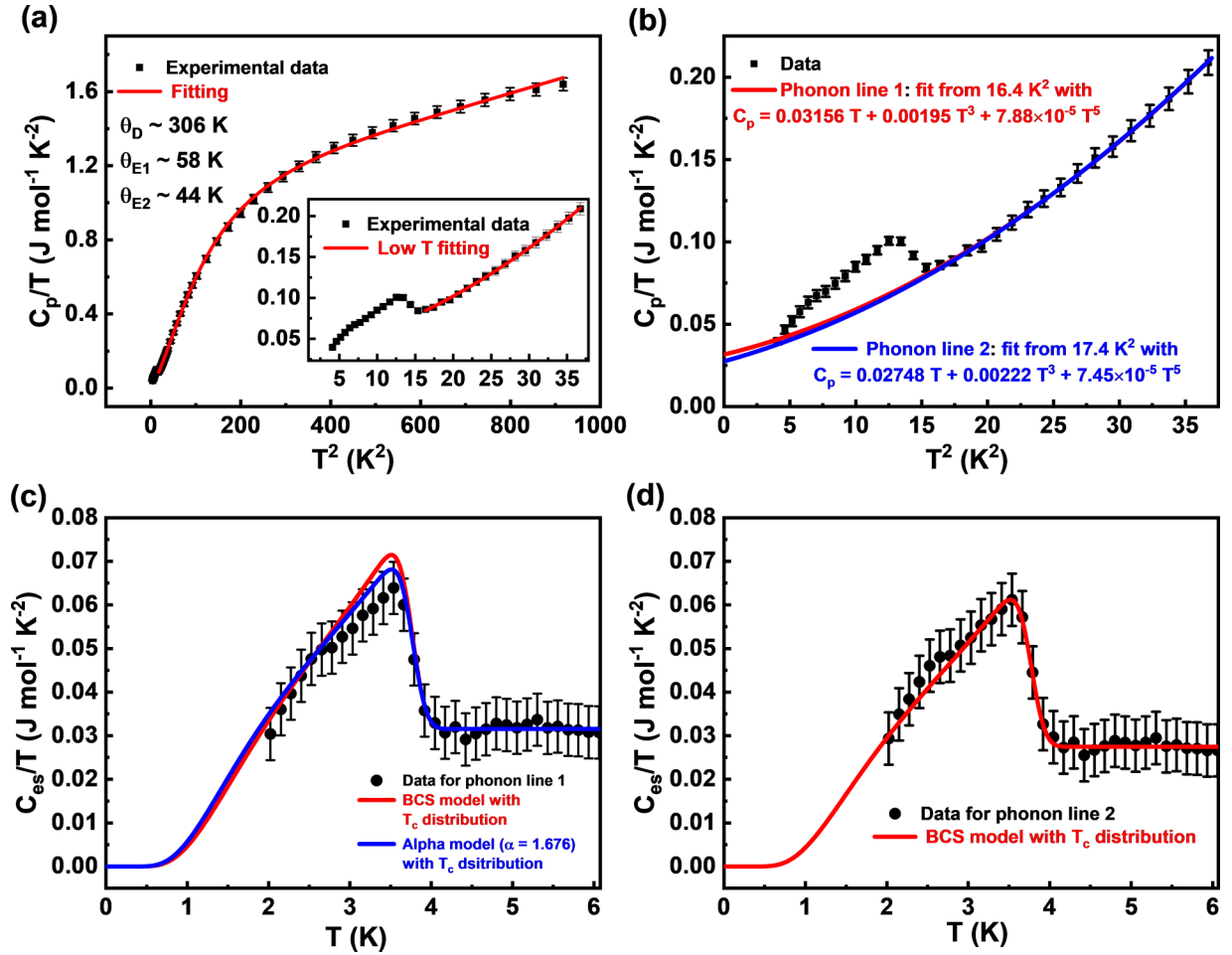


FIG. 3. (a) C_p/T vs T^2 plot of the normal state of PbMo_6Se_8 fitted with Eq. (6) with $\gamma = 31.56 \text{ mJ mol}^{-1} \text{ K}^{-2}$ and observation of low-energy soft phonon modes. The inset shows the enlarged scale low T fitting of C_p/T vs T^2 . (b) Low-temperature normal state specific heat was fitted with two closely spaced distinct phonon lines fitted with $C_p = \gamma T + \beta T^3 + \delta T^5$ from 16.4 to 37 K^2 (phonon line 1) and from 17.4 to 37 K^2 (phonon line 2). BCS model fitting is shown in (c) and (d) for two-phonon channels incorporating a Gaussian T_c distribution with Eq. (7) by integration, at mean $T_{c,m} = 3.77$ up to 3σ . We derived an alpha model with α set as a free parameter, yielding a value of 1.676, which closely aligns with the BCS limit of 1.764.

specific-heat data in the temperature range 4–30 K:

$$\frac{C_p}{T} = \gamma + \beta T^2 + 3R \sum_i \delta_i \frac{\left(\frac{\theta_{E_i}}{T}\right)^2 e^{\frac{\theta_{E_i}}{T}}}{T(e^{\frac{\theta_{E_i}}{T}} - 1)^2}, \quad (6)$$

where δ_i is the fractional contribution of the low-lying Einstein mode, and E_i is the i th level Einstein energy keeping the γ value fixed ($31.56 \pm 6.13 \text{ mJ mol}^{-1} \text{ K}^{-2}$) as obtained from the earlier fit of $\frac{C_p}{T}$ versus T^2 from a T range of 4–6 K. We obtained $\beta = 0.930 \pm 0.026 \text{ mJ mol}^{-1} \text{ K}^{-4}$, $\delta_1 = 1.17 \pm 0.03$, $\theta_{E_1} = 58.36 \pm 0.96 \text{ K}$, $\delta_2 = 0.071 \pm 0.008$, $\theta_{E_2} = 44.09 \pm 0.83 \text{ K}$ from Eq. (6). The Debye temperature obtained from the β term of Eq. (6) is given by $\theta_D = \left(\frac{12NR\pi^4}{5\beta}\right)^{1/3}$, where N = total number of atoms in a unit cell = 15 for the case of our sample = $315.3 \pm 3.0 \text{ K}$. The effective Debye temperature was calculated as $\theta_D^{\text{eff}} = \theta_D[(N - \delta_1 - \delta_2)/N]^{1/3} = 306.3 \pm 3.2 \text{ K}$ after consideration of Einstein modes in the system. The effective Debye temperature comes close in both approximations. The estimated Einstein modes (θ_E) obtained from the fitting are much lower than the

Debye temperature (θ_D^{eff}), which indicates the presence of low-energy phonon modes in the system. Theoretical studies on the isostructural compound PbMo_6S_8 have revealed flat bands in phonon dispersion [27]. We stipulate the same reason for obtaining much lower Einstein modes than that of the Debye modes in PbMo_6Se_8 . However, theoretical studies on it are required to understand the thermodynamic properties in detail.

To investigate the superconducting gap value and related parameters precisely, we have calculated $C_e/\gamma T$ by subtracting two different phononic contributions obtained from the normal state specific-heat fitting of two different temperature ranges of value from 16.4 to 37 K^2 and from 17.4 to 37 K^2 , named phonon line 1 and phonon line 2, shown in Fig. 3(b). For a BCS superconductor [16,28,29], the superconducting entropy [$S_{\text{es}}(t)$] and the specific heat (C_{es}) are given by the following equations:

$$\begin{aligned} \frac{S_{\text{es}}(t)}{\gamma T_c} &= -\frac{3\alpha}{\pi^2} \int_0^\infty [f_x \ln f_x - (1 - f_x) \ln(1 - f_x)] dx, \\ \frac{C_{\text{es}}}{\gamma T_c} &= t \frac{d}{dt} \left(\frac{S_{\text{es}}(t)}{\gamma T_c} \right), \end{aligned} \quad (7)$$

where $t = \frac{T}{T_c}$ and $f_x = [\exp \alpha t^{-1}(x^2 + \delta^2)^{1/2} + 1]^{-1}$, the superconducting energy gap (Δ) is given by $\Delta = \alpha k_B T_c$, and for an ideal s -wave BCS superconductor, $\alpha = 1.764$.

The subtraction of the phonon's contribution of phonon line 1 and phonon line 2 from the total specific heat (C_p) data has generated two closely spaced data sets, as illustrated in Figs. 3(c) and 3(d). We obtained a reasonable BCS model for both data sets after incorporating a Gaussian distribution in T_c with Eq. (7). The incorporation of the Gaussian distribution of T_c was necessary to account for the broadening of the transition temperature. In both data sets, the specific-heat jump $\frac{\Delta C_c}{\gamma T_c}$ is determined to be 1.26 (phonon line 1) and 1.22 (phonon line 2) after employing the optimized T_c distribution with $T_{c,m} = 3.77$ K and $\Delta T = 0.8$ K. This values are slightly lower than the BCS limit of 1.43. This reduction is associated with the broadening of T_c and might lead to 1.43 for a sharp transition. Further, for the data set of channel 1, we extended the BCS model to the α model (with the same Gaussian distribution as stated earlier shown by solid blue line in Fig. 3(c)) by keeping it as a free parameter, and we obtained $\alpha = 1.676$, which is a bit reduced but close to the BCS limit (95% of 1.764). We achieved $\alpha = 1.732$ (98% of 1.764) for phonon line 2. However, it has not been depicted in the Fig. 3(d) as it closely approached the BCS limit, resulting in negligible visual distinction. Therefore, these results suggest a potential BCS superconductivity in PbMo₆Se₈.

Nevertheless, the isostructural PbMo₆S₈ has a multigap superconductivity reported earlier through STM studies [12]. Unfortunately, as we do not have any low-temperature data points, we are unable to comment on this direction. However, a detailed μ SR investigation is required to comment on the superconducting gap structure of PbMo₆Se₈, which is beyond the scope of this study.

D. Superconducting parameters

By using the value of $\mu_0 H_{c2}(0) = 4.62 \pm 0.02$ T, we have calculated the coherence length $\xi_{GL}(0)$ using the formula $\xi_{GL}(0) = (\frac{\Phi_0}{2\pi H_{c2}(0)})^{1/2}$, where Φ_0 is the flux quantum, $\frac{h}{2e}$ (h = Planck's constant, e = electronic charge). We obtained a value of $\xi_{GL}(0) = 8.43 \pm 0.02$ nm, which is 12 times the dimensions of a single unit cell suggesting a long scale phase synchronization of Cooper pairs [24]. The value of superconducting penetration depth $\lambda_{GL}(0)$, calculated using the equation $\mu_0 H_{c1}(0) = \frac{\phi_0}{4\pi \lambda_{GL}^2} \ln \frac{\lambda_{GL}}{\xi_{GL}}$, is 252.9 ± 0.6 nm. We obtained the value of the Ginzburg-Landau parameter $\kappa = \frac{\lambda_{GL}}{\xi_{GL}} \approx 30$, which is $\gg \frac{1}{\sqrt{2}}$ (limit for type I superconductor) suggesting PbMo₆Se₈ is a type II superconductor [16]. The thermodynamic critical field $\mu_0 H_c$, which is a measure of superconducting condensation energy, measured from the relation $H_{c1} H_{c2} = H_c^2 \ln \kappa$, is 108 ± 1 mT. Above $H_{c2}(T)$ the superconductivity is lost completely by breaking of Cooper pairs into normal electrons. For an ideal BCS superconductor, the orbital critical field H_{c2}^{orb} is given by the Werthamer-Helfand-Hohenberg (WHH) formula [30] in the following equation:

$$H_{c2}^{orb} = -AT_c \left(\frac{dH_{c2}}{dT} \right)_{T=T_c}, \quad (8)$$

where $A = 0.69$ and 0.73 for dirty and clean limits of superconductivity, respectively. We obtained $\mu_0 \frac{dH_{c2}}{dT} = -1.38$ T K⁻¹ from a linear fit of the resistivity data of H_{c2} versus T . From this, we obtained $\mu_0 H_{c2}^{orb} = 3.62 \pm 0.03$ or 3.83 ± 0.03 T for the dirty and clean limit of superconductivity, respectively. If we consider only the spin paramagnetic effect, the Pauli critical field can be written as $H_P = \frac{\Delta}{\sqrt{2}\mu_B}$, where Δ is the superconducting gap value. We estimate the electron-phonon coupling constant λ_{ep} by the McMillan formula [16,30] given by the following equation:

$$\lambda_{ep} = \frac{1.04 + \mu^* \ln(\Theta_D/1.45T_c)}{(1 - 0.62\mu^*) \ln(\Theta_D/1.45T_c) - 1.04}, \quad (9)$$

where $\mu^* = 0.13$ is Coulomb's pseudopotential that is widely used for intermetallic superconductors. We obtained $\lambda_{ep} = 0.59 \pm 0.04$, which indicates a moderately strong electron-phonon coupling constant. We have also calculated the density of states at the Fermi level $N(\epsilon_F)$ from the relation $N(\epsilon_F) = \frac{3\gamma}{\pi^2 k_B^2 (1 + \lambda_{ep})} = 8.39 \pm 0.44$ states eV⁻¹ f.u.⁻¹. To compare the pair-breaking mechanism among the orbital limiting effect and Pauli paramagnetic limit [31,32], the Pauli paramagnetic field H_P can be calculated as $H_P = \frac{\Delta}{\sqrt{2}\mu_B}$, however for a strongly coupled superconductor it can be referred to [33] as H_P^{str} and can be obtained by the equation $H_P^{str} = \frac{\Delta}{\sqrt{2}\mu_B} (1 + \lambda_{ep})$. We obtained $\mu_0 H_P^{str} = 11.12$ T (taking $\Delta = \Delta_{BCS} = 1.764 k_B T_{c,m}$), which is much higher than the orbital critical field. Using this orbital critical field and the strongly coupled Pauli paramagnetic field, we obtained the Maki parameter [34] expressed as $\alpha_M = \sqrt{2} \frac{H_{c2}^{orb}}{H_P^{str}}$, which turns out to be 0.46 or 0.48 for the dirty and clean limit of superconductor, respectively. If the Pauli paramagnetic limiting field (H_P^{str}) is less than and close to the value of the orbital limiting field (H_{c2}^{orb}), then the pair-breaking mechanism can be attributed to the Pauli paramagnetic effect, but if the orbital limiting field (H_{c2}^{orb}) is much lower than the Pauli limiting field (H_P^{str}), then the Cooper pair breaking mechanism is solely dominated by the orbital limiting field. The obtained value of $\alpha_M \ll 1$ indicates the breaking of Cooper pairs in PbMo₆Se₈ is governed by the orbital limiting effect [24]. All the superconducting parameters are listed in Table I.

E. Vortex phase

The M versus $\mu_0 H$ loops shown in Figs. 2(b) and 2(c) suggest that beyond the Meissner state, the system undergoes different vortex phases at different magnetic field regions, which can be associated with multiple anomalies in the M versus $\mu_0 H$ data shown Fig. 2(c). The different vortex phase transition is associated with magnetic fields $\mu_0 H_m$, $\mu_0 H_{SP}$, and $\mu_0 H_{irr}$ called first minima, secondary peak, and irreversibility field between increasing and decreasing magnetic field lines, respectively. From full-range M versus $\mu_0 H$ data at 1.9 K shown in Fig. 2(b), we calculated the critical current density from Bean's model [35,36] as $J_c = 20 \frac{\Delta M}{a(1-a/3b)} \approx 2 \times 10^5$ A cm², which is quite large and comparable to LiFeAs single crystals [37] and which is close to Ba-122 and 1111 superconductors where $J_c \approx 10^6$ A cm² [4,18,19,37–40]. With the so far obtained data we have constructed the vortex phase

TABLE I. Superconducting parameters.

Parameter	Value
$T_{c,m}$	3.77 K
RRR	3.65
γ	31.56 mJ mol ⁻¹ K ⁻²
θ_D	306.3 K
θ_{E1}	58.36 K
θ_{E2}	44.09 K
λ_{ep}	0.59
$N(\epsilon_F)$	8.39 states eV ⁻¹ f.u. ⁻¹
$\mu_0 H_{c1}(0)$	8.588 mT
$\mu_0 H_{c2}(0)$	4.62 T
$\mu_0 H_m(0)$	36.918 mT
$\mu_0 H_{SP}(0)$	136.282 mT
$\mu_0 H_{irr}(0)$	3.72 T
$\xi_{GL}(0)$	8.43 nm
$\lambda_{GL}(0)$	252.9 nm
κ	30
$\mu_0 H_c$	108 mT
$\mu_0 H_P^{str}$	11.12 T
$\mu_0 H_{c2}^{orb}$	3.62 T (dirty) or 3.83 T (clean)
α_M	0.46 (dirty) or 0.48 (clean)

diagram of the system in this section. Figure 2(b) (inset) shows the evolution of decreasing $\mu_0 H_{SP}$ with increasing T , which discards the possibility of originating a secondary peak from the order-disorder vortex phase transition [17,41,42]. According to the elastic creep to plastic creep phase transition model, if $\mu_0 H_{SP}$ is the associated point of transition, it should follow a temperature dependency of $\mu_0 H_{SP}(T) = \mu_0 H_{SP}(0)(1 - t^4)^{1.4}$, where $t = \frac{T}{T_c}$. Though we observed a decrease of $\mu_0 H_{SP}$ with increasing T , this equation did not fit with our experimental data, suggesting that this model may not be ideal for explaining the origin of a secondary peak as observed earlier in few Fe-based superconductors such as LiFeAs [37,43] and Ba(Fe_{0.97}Co_{0.07})₂As₂ [18]. As the phase transition cannot be described by the elastic to plastic creep transition evident from dc magnetization studies, we are calling the states “elastic creeplike state,” “plastic creeplike state,” and we have fitted the data with the empirical model used earlier for several similar systems, such as high- T_c cuprates and Fe-based superconductors [37,40,41,43] as $\mu_0 H_{SP}(T) = \mu_0 H_{SP}(0)(1 - t)^n$ obtaining $\mu_0 H_{SP}(0) = 136.282 \pm 3.715$ mT, $n = 1.01 \pm 0.04$. From magnetization data, the bifurcation temperature (T) of field-cooled line (FC) and zero-field-cooled (ZFC) line was recorded at a different field ($\mu_0 H_{irr}$) and was plotted with the equation $H_{irr}(T) = H_{irr}(0)(1 - t)^n$ obtaining a value of $\mu_0 H_{irr}(0) = 3.72 \pm 0.40$ T and $n = 1.20 \pm 0.09$. The fitted value of H_{irr} at 1.9 K, i.e., $\mu_0 H_{irr}^{fit}(1.9 \text{ K})$, is ≈ 1.62 T, which is close to the experimental value of FC-ZFC bifurcation of increasing and decreasing M versus $\mu_0 H$ cycle at 1.9 K. The fitted value of $\mu_0 H_{irr}^{data}(1.9 \text{ K})$ is ≈ 1.58 T, shown in Fig. 2(b), inset. This vortex liquid state can be referred to as the movement of the vortices or the melting of the vortices. The phase between $\mu_0 H_{irr}$ and $\mu_0 H_{c2}$ is referred to as the “vortex liquid state.” The crossover from “elastic creeplike state” to “vortex solid state” can be associated with H_m fitted with the

empirical equation as $\mu_0 H_m(T) = \mu_0 H_m(0)(1 - t)^n$ obtaining $\mu_0 H_m(0) = 36.918 \pm 0.556$ mT and $n = 0.58 \pm 0.01$. The $\mu_0 H_{c1}(T)$ line differentiates between the “Meissner state” and the “vortex solid state” state obtained from the fitting of Eq. (1). To get an insight about the origin of multiple vortex phase crossover, we have investigated detailed vortex dynamics by means of magnetic field (H) dependency of the vortex pinning energy (U) by magnetic relaxation experiments [44,45]. When we apply an external magnetic field to a type II superconductor beyond its Meissner state, the magnetic field lines start to enter the SC by creating a vortex state. As an outcome, these magnetic field lines exert Lorentz force on the vortices causing their movement which is attributed to the nonequilibrium special arrangements causing change in $M(t)$ with time (t). Magnetization follows a logarithmic dependency on time and is associated with some energy costs. According to the Anderson model [40,46], the dependency of $M(t)$ over time t at a particular temperature T can be expressed by the following equation:

$$M(H, t) = M_0(H) \left[1 - \frac{k_B T}{U_0(H)} \ln \left(\frac{t}{t_0} \right) \right], \quad (10)$$

where $M_0(H)$ is initial magnetization at $t \rightarrow 0$, $U_0(H)$ is the energy barrier to create a vortex, which is associated with Lorentz force (pinning energy), and t_0 is the characteristic time. We obtained very slow relaxation with $\approx 1.5\%$ change in $M(H)$ at 2 K for 62.5 mT magnetic field for 7200 s, which is much lower than the observed cuprates and Fe-based superconductors [41,45]. We have obtained the characteristic timescale $t_0 \approx 10$ s, which is much higher than that of a typical type II superconductor ($\approx 10^{-6}$ s). The rate of relaxation calculated as $S = -\frac{d(\ln M(t))}{d(\ln t)}$ turns out to be very low, ≈ 0.005 (unitless quantity), which is even lower than Ba-122 and 1111 materials where $S > 0.01$ [18,39,47]. We have studied the magnetic field dependency of $U_0(H)$ at 2 K obtained from the relaxation measurements shown in the inset of Fig. 4(b). This shows an anomaly near $\mu_0 H \approx 27.5$ mT given in Fig. 4(b), which is close to $\mu_0 H_m$ suggesting a vortex crossover near this magnetic field $\mu_0 H \approx 27.5$ mT. $U_0(H)$ decreases monotonically after 27.5 mT suggesting that the cost of energy for the magnetic field to get pinned starts decreasing and this is physically valid from the context of type II BCS superconductors. However, we did not see any anomaly in this plot around $\mu_0 H_{SP} \approx 62.5$ mT, which also suggests that the origin of a secondary peak cannot ideally be described by the elastic to plastic creep phase transition model. There has been no theoretical model so far to explain the origin of these kinds of vortex dynamics. These kinds of unusual properties have also been found in a LiFeAs single crystal by Pramanik *et al.* [37]. However, many more studies in a single crystal are required in detail to understand the origin of it. We guess that both anomalies in the U_0 versus $\mu_0 H$ plot are associated with $\mu_0 H_m$ and $\mu_0 H_{SP}$ and have shifted to lower H values in association with some unknown phase crossover mechanism.

In summary, we have established a $\mu_0 H$ - T phase diagram based on the magnetization and resistivity studies classifying different superconducting phases such as the Meissner state, vortex solid, elastic creeplike state, plastic creeplike state, vortex liquid state, and the normal state shown in Fig. 4(a).

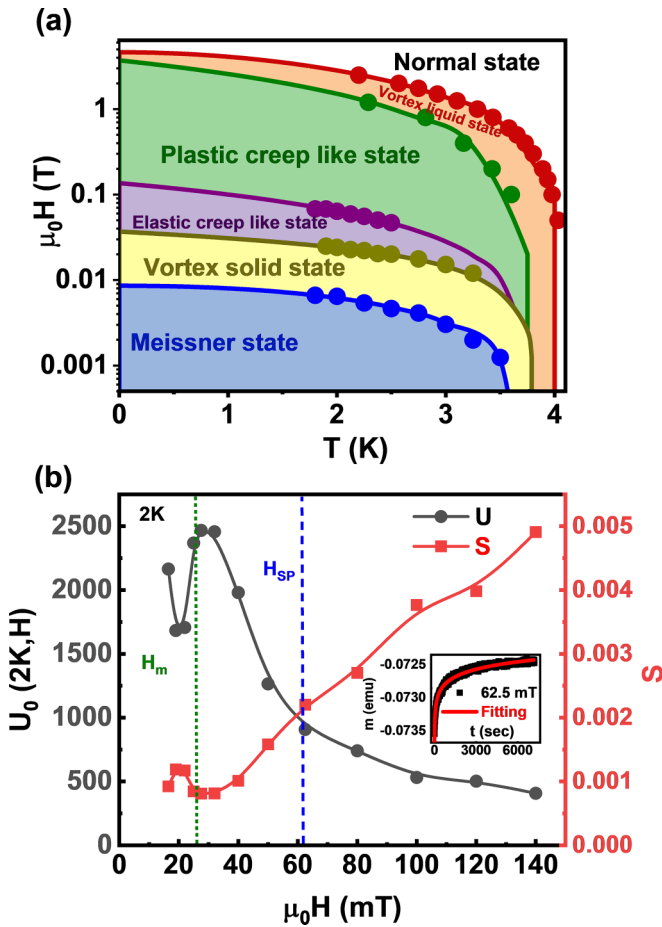


FIG. 4. (a) The $\mu_0 H$ - T phase diagram of superconductor PbMo_6Se_8 classifying Meissner state, vortex solid, elastic solid, plastic solid, vortex liquid like states and the normal state obtained from magnetization data and resistivity data. (b) The magnetic field dependency of pinning energy U_0 at 2 K obtained from the magnetic relaxation. The right side of the graph is represented as the relaxation rates.

The detailed investigation of the vortex state from isothermal magnetization, magnetic relaxation, and magnetic field dependency of pinning energy suggests an unconventional

vortex state whose mechanism is not theoretically developed yet and was observed in a few materials earlier, e.g., LiFeAs [37], $\text{Ba}(\text{Fe}_{1-x}\text{Co}_x)_2\text{As}_2$ [18], $\text{SmFeAsO}_{1-x}\text{F}_x$ [47–49], and $\text{CaKFe}_4\text{As}_4$ [50], which suggests that many more studies on this system are required both from an experimental and theoretical point of view to understand the mechanism carefully. However, irrespective of the origin, this Chevrel phase compound demands much more attention to understand its unconventional vortex state and fishtail effect, which is probably one of the rarest cases apart from the class of cuprates and Fe-based layered unconventional superconductors.

IV. CONCLUSION

In conclusion, we have established the Chevrel phase compound PbMo_6Se_8 as a type-II superconductor with $T_c = 3.8$ K with $\mu_0 H_{c2}(0) \approx 4.5$ T, which is almost 3.7 and 14 times lower than the isostructural PbMo_6S_8 , respectively. The specific-heat data exhibit characteristics reminiscent of BCS superconductivity in PbMo_6Se_8 . The unconventional vortex state was evident from the unusual fishtail effect, and the nonmonotonous magnetic field dependencies of the vortex pinning obtained from the magnetic relaxation experiments. Further, a detailed multivortex phase diagram was constructed based on magnetic, resistive properties. Hence, we believe this study will accelerate the investigation of Chevrel phase compounds in the context of the unconventional vortex state and multivortex phase crossover. Nevertheless, microscopic investigation through imaging of magnetic flux lines and probing the SC ground state through μSR is required to understand the origin of this unconventionality.

ACKNOWLEDGMENTS

The authors thank Sheikh Saqr Lab (SSL), International Centre for Materials Science (ICMS), and School of Advanced Materials (SAMat) at Jawaharlal Nehru Centre for Advanced Scientific Research (JNCASR) for various experimental facilities. S.B. thanks Council of Scientific & Industrial Research (CSIR), India for the fellowship of Grant No. 09/733(0286)/2020-EMR-I. S.G. thanks JNCASR for the fellowship. S.B. thanks Ritam Chakraborty and Kartik Panda at JNCASR for fruitful discussions.

[1] R. Chevrel, M. Sergent, and J. Prigent, Sur de nouvelles phases sulfurées ternaires du molybdène, *J. Solid State Chem.* **3**, 515 (1971).
 [2] R. Chevrel and M. Sergent, *Chemistry and Structure of Ternary Molybdenum Chalcogenides* (Springer, Berlin, 1982), pp. 25–86.
 [3] R. N. Shelton, R. W. McCallum, and H. Adrian, Superconductivity in rare earth molybdenum selenides, *Phys. Lett. A* **56**, 213 (1976).
 [4] W. A. Fertig, D. C. Johnston, L. E. DeLong, R. W. McCallum, M. B. Maple, and B. T. Matthias, Destruction of superconductivity at the onset of long-range magnetic order in the compound ErRh_4B_4 , *Phys. Rev. Lett.* **38**, 987 (1977).

[5] W. Goldacker, G. Rimikis, E. Seibt, and R. Flukiger, Improved $\text{Sn}_{1.2}\text{Mo}_6\text{S}_8$ wire preparation technique, *IEEE Trans. Magn.* **27**, 1779 (1991).
 [6] T. C. Willis, P. D. Jablonski, D. C. Larbalestier, S. Even-Boudjada, R. Chevrel, and M. Sergent, Hot isostatic pressing of Chevrel phase bulk and hydrostatically extruded wire samples, *IEEE Trans. Appl. Supercond.* **5**, 1209 (1995).
 [7] H. D. Ramsbottom and D. P. Hampshire, Improved critical current density and irreversibility line in HIP'ed Chevrel phase superconductor PbMo_6S_8 , *Phys. C* **274**, 295 (1997).
 [8] B. Seeber, M. Decroux, and Ø. Fischer, Status and prospects of superconducting Chevrel phase wires for high magnetic field applications, *Phys. B* **155**, 129 (1989).

- [9] Y. Kubo, K. Yoshizaki, and Y. Hashimoto, Superconducting properties of Chevrel-phase PbMo_6S_8 , *Synth. Met.* **18**, 851 (1987).
- [10] R. Horyń, Phase relations in the Pb-Mo-Se ternary system at 1323 K and the superconductivity of the alloys, *J. Less Common Metals* **98**, 1 (1984).
- [11] C. Dubois, A. P. Petrovic, G. Santi, C. Berthod, A. A. Manuel, M. Decroux, Ø. Fischer, M. Potel, and R. Chevrel, Node-like excitations in superconducting PbMo_6S_8 probed by scanning tunneling spectroscopy, *Phys. Rev. B* **75**, 104501 (2007).
- [12] A. P. Petrovic, R. Lortz, G. Santi, C. Berthod, C. Dubois, M. Decroux, A. Demuer, A. B. Antunes, A. Paré, D. Salloum, P. Gougeon, M. Potel, and Ø. Fischer, Multiband superconductivity in the Chevrel phases SnMo_6S_8 and PbMo_6S_8 , *Phys. Rev. Lett.* **106**, 017003 (2011).
- [13] J. R. Carvajal, *Abstract of the Satellite Meeting on Powder Diffraction of the XV Congress of the IUCr* (IUCr, Toulouse, France, 1990), Vol. 127.
- [14] F. S. Delk and M. J. Sienko, Relationship between superconductivity, magnetic susceptibility, and crystal structure in the pseudobinary system PbMo_6S_8 - PbMo_6Se_8 , *Inorg. Chem.* **19**, 1352 (1980).
- [15] R. Prozorov and V. G. Kogan, Effective demagnetizing factors of diamagnetic samples of various shapes, *Phys. Rev. Appl.* **10**, 014030 (2018).
- [16] M. Tinkham, *Introduction to Superconductivity*, 2nd ed. (Dover, Mineola, New York, 2004).
- [17] Y. Radzyner, A. Shaulov, Y. Yeshurun, I. Felner, K. Kishio, and J. Shimoyama, Anisotropic order-disorder vortex transition in $\text{La}_{2-x}\text{Sr}_x\text{CuO}_4$, *Phys. Rev. B* **65**, 214525 (2002).
- [18] R. Prozorov, N. Ni, M. A. Tanatar, V. G. Kogan, R. T. Gordon, C. Martin, E. C. Blomberg, P. P. M. Wang, J. Q. Yan, S. L. Bud'ko, and P. C. Canfield, Vortex phase diagram of $\text{Ba}(\text{Fe}_{0.93}\text{Co}_{0.07})_2\text{As}_2$ single crystals, *Phys. Rev. B* **78**, 224506 (2008).
- [19] S. Salem-Sugui, L. Ghivelder, A. D. Alvarenga, L. F. Cohen, H. Luo, and X. Lu, Fishtail and vortex dynamics in the Ni-doped iron pnictide $\text{BaFe}_{1.82}\text{Ni}_{0.18}\text{As}_2$, *Phys. Rev. B* **84**, 052510 (2011).
- [20] D. A. Mayoh, J. A. T. Barker, R. P. Singh, G. Balakrishnan, D. M. K. Paul, and M. R. Lees, Superconducting and normal-state properties of the noncentrosymmetric superconductor Re_6Zr , *Phys. Rev. B* **96**, 064521 (2017).
- [21] H. Wiesmann, M. Gurvitch, H. Lutz, A. Ghosh, B. Schwarz, M. Strongin, P. B. Allen, and J. W. Halley, Simple model for characterizing the electrical resistivity in $A - 15$ superconductors, *Phys. Rev. Lett.* **38**, 782 (1977).
- [22] Z. Fisk and G. W. Webb, Saturation of the high-temperature normal-state electrical resistivity of superconductors, *Phys. Rev. Lett.* **36**, 1084 (1976).
- [23] V. Sankaranarayanan, G. Rangarajan, and R. Srinivasan, Normal-state electrical resistivity of Chevrel-phase superconductors of the type $\text{Cu}_{1.8}\text{Mo}_6\text{S}_{8-y}\text{Se}_y$, $0 \ll y \ll 8$, *J. Phys. F* **14**, 691 (1984).
- [24] M. Naskar, S. Ash, D. P. Panda, C. K. Vishwakarma, B. K. Mani, A. Sundaresan, and A. K. Ganguli, Experimental and first-principles studies on superconductivity in noncentrosymmetric La_3Se_4 , *Phys. Rev. B* **105**, 014513 (2022).
- [25] R. Lortz, Y. Wang, U. Tutsch, S. Abe, C. Meingast, P. Popovich, W. Knafo, N. Shitsevalova, Y. B. Paderno, and A. Junod, Superconductivity mediated by a soft phonon mode: Specific heat, resistivity, thermal expansion, and magnetization of YB_6 , *Phys. Rev. B* **73**, 024512 (2006).
- [26] S. Roychowdhury, M. K. Jana, J. Pan, S. N. Guin, D. Sanyal, U. V. Waghmare, and K. Biswas, Soft phonon modes leading to ultralow thermal conductivity and high thermoelectric performance in AgCuTe , *Angew. Chem. Int. Ed.* **57**, 4043 (2018).
- [27] G. Marini, A. Sanna, C. Pellegrini, C. Bersier, E. Tosatti, and G. Profeta, Superconducting Chevrel phase PbMo_6S_8 from first principles, *Phys. Rev. B* **103**, 144507 (2021).
- [28] J. Singh, A. Jayaraj, D. Srivastava, S. Gayen, A. Thamizhavel, and Y. Singh, Possible multigap type-I superconductivity in the layered boride RuB_2 , *Phys. Rev. B* **97**, 054506 (2018).
- [29] H. Padamsee, J. E. Neighbor, and C. A. Shiffman, Quasiparticle phenomenology for thermodynamics of strong-coupling superconductors, *J. Low Temp. Phys.* **12**, 387 (1973).
- [30] N. R. Werthamer, E. Helfand, and P. C. Hohenberg, Temperature and purity dependence of the superconducting critical field, H_{c2} . III. Electron spin and spin-orbit effects, *Phys. Rev.* **147**, 295 (1966).
- [31] B. S. Chandrasekhar, A note on the maximum critical field of high - field superconductors, *Appl. Phys. Lett.* **1**, 7 (1962).
- [32] A. M. Clogston, Upper limit for the critical field in hard superconductors, *Phys. Rev. Lett.* **9**, 266 (1962).
- [33] M. Schossmann and J. P. Carbotte, Pauli limiting of the upper critical magnetic field, *Phys. Rev. B* **39**, 4210 (1989).
- [34] K. Maki, Effect of Pauli paramagnetism on magnetic properties of high-field superconductors, *Phys. Rev.* **148**, 362 (1966).
- [35] C. P. Bean, Magnetization of hard superconductors, *Phys. Rev. Lett.* **8**, 250 (1962).
- [36] C. P. Bean, Magnetic behavior of high-field superconductors, *J. Appl. Phys.* **35**, 759 (1964).
- [37] A. K. Pramanik, L. Harnagea, C. Nacke, A. U. B. Wolter, S. Wurmehl, V. Kataev, and B. Büchner, Fishtail effect and vortex dynamics in LiFeAs single crystals, *Phys. Rev. B* **83**, 094502 (2011).
- [38] D. L. Sun, Y. Liu, and C. T. Lin, Comparative study of upper critical field H_{c2} and second magnetization peak H_{sp} in hole- and electron-doped BaFe_2As_2 superconductor, *Phys. Rev. B* **80**, 144515 (2009).
- [39] K. Gofryk, A. S. Sefat, M. A. McGuire, B. C. Sales, D. Mandrus, J. D. Thompson, E. D. Bauer, and F. Ronning, Doping-dependent specific heat study of the superconducting gap in $\text{Ba}(\text{Fe}_{1-x}\text{Co}_x)_2\text{As}_2$, *Phys. Rev. B* **81**, 184518 (2010).
- [40] B. Shen, P. Cheng, Z. Wang, L. Fang, C. Ren, L. Shan, and H. H. Wen, Flux dynamics and vortex phase diagram in $\text{Ba}(\text{Fe}_{1-x}\text{Co}_x)_2\text{As}_2$ single crystals revealed by magnetization and its relaxation, *Phys. Rev. B* **81**, 014503 (2010).
- [41] B. Khaykovich, E. Zeldov, D. Majer, T. W. Li, P. H. Kes, and M. Konczykowski, Vortex-lattice phase transitions in $\text{Bi}_2\text{Sr}_2\text{CaCu}_2\text{O}_8$ crystals with different oxygen stoichiometry, *Phys. Rev. Lett.* **76**, 2555 (1996).
- [42] D. Giller, A. Shaulov, R. Prozorov, Y. Abulafia, Y. Wolfus, L. Burlachkov, Y. Yeshurun, E. Zeldov, V. M. Vinokur, J. L. Peng, and R. L. Greene, Disorder-induced transition to entangled vortex solid in Nd-Ce-Cu-O crystal, *Phys. Rev. Lett.* **79**, 2542 (1997).
- [43] P. P. M. Wang, M. A. Tanatar, B. Lee, S. Khim, K. H. Kim, and R. Prozorov, Magnetic-field-dependent pinning potential in

- LiFeAs superconductor from its Campbell penetration depth, *Phys. Rev. B* **84**, 060509(R) (2011).
- [44] D. I. Khomskii and A. Freimuth, Charged vortices in high temperature superconductors, *Phys. Rev. Lett.* **75**, 1384 (1995).
- [45] Y. Yeshurun, A. P. Malozemoff, and A. Shaulov, Magnetic relaxation in high-temperature superconductors, *Rev. Mod. Phys.* **68**, 911 (1996).
- [46] P. W. Anderson and Y. B. Kim, Hard superconductivity: Theory of the motion of Abrikosov flux lines, *Rev. Mod. Phys.* **36**, 39 (1964).
- [47] H. Yang, C. Ren, L. Shan, and H. H. Wen, Magnetization relaxation and collective vortex pinning in the Fe-based superconductor $\text{SmFeAsO}_{0.9}\text{F}_{0.1}$, *Phys. Rev. B* **78**, 092504 (2008).
- [48] C. Senatore, R. Flükiger, M. Cantoni, G. Wu, R. H. Liu, and X. H. Chen, Upper critical fields well above 100 T for the superconductor $\text{SmFeAsO}_{0.85}\text{F}_{0.15}$ with $T_c = 46$ K, *Phys. Rev. B* **78**, 054514 (2008).
- [49] P. J. W. Moll, R. Puzniak, F. Balakirev, K. Rogacki, J. Karpinski, N. D. Zhigadlo, and B. Batlogg, High magnetic-field scales and critical currents in $\text{SmFeAs}(\text{O}, \text{F})$ crystals, *Nat. Mater.* **9**, 628 (2010).
- [50] S. J. Singh, M. Bristow, W. R. Meier, P. Taylor, S. J. Blundell, P. C. Canfield, and A. I. Coldea, Ultrahigh critical current densities, the vortex phase diagram, and the effect of granularity of the stoichiometric high- T_c superconductor $\text{CaKFe}_4\text{As}_4$, *Phys. Rev. Mater.* **2**, 074802 (2018).